FINITE ELEMENT SIMULATION OF DEEP DRAWING WITH INITIAL AND INDUCED ANISOTROPY

Tudor Balan, LPMM, ENSAM Metz, 4 rue A. Fresnel, 57078 Metz Cedex, France
Farid Abed-Meraim, LPMM, ENSAM Metz, 4 rue A. Fresnel, 57078 Metz Cedex, France
Badis Haddag, LPMM, ENSAM Metz, 4 rue A. Fresnel, 57078 Metz Cedex, France

Abstract

Deep drawing is a forming process widely used to obtain parts of suited shape from sheets initially flat. These sheets are obtained generally by rolling and thus present an initial orthotropic anisotropy. Several behaviour models have been proposed to predict their induced anisotropy evolution at large strains. The models frequently used in finite element simulation are the phenomenological ones. This work concerns the prediction of the macroscopic behaviour of thin sheets and of the final part properties in deep drawing. A dislocation-based micro-structural hardening model taking into account the strain-path induced anisotropy is considered, together with anisotropic yield surfaces. The numerical integration of the constitutive equations in order to implement the model in finite element codes is discussed. Consequently, several explicit schemes for the integration of the model (forward Euler, 2nd and 4th order Runge-Kutta) are implemented. In order to asses the relative accuracy of these schemes, we compare experimental and simulated rheological tests for different grades of steel sheet. Finally, finite element computations are performed to predict the spring-back and its dependence on deep drawing process parameters.
Key words: finite element simulation, anisotropy, spring-back, time integration

1. Introduction

The material model is clearly recognised as an important factor influencing the accuracy of the numerical simulations in sheet forming. During the last decades, numerous material models have been proposed, both for the modelling of the yield surface and of the hardening behaviour. Yet, these models are available much later in the commercial finite element codes and very often the user has to make their numerical implementation himself. This is a difficult task when an accurate implementation is desired. Moreover, any new model requires very often the development of the complete implementation.

The aim of this work is twofold. First, a general framework is chosen for the material model. Modern, physically-based hardening laws are shown to fall into this framework (Section 2). Explicit, Runge-Kutta type integration schemes are used for its numerical implementation in the FE code Abaqus (subsection 3.1). Rheological test simulations are used to asses the interest of such a constitutive model (subsections 3.2 and 3.3). The finite element spring-back predictions are analysed for two different sheet steels (subsection 3.4).

2. Material model considerations

A material description based on rate equations must respect the principle of objectivity. In finite element implementations, the most commonly used technique is to integrate the rate equations in a frame that rotates with the spin $\boldsymbol{W}$ (skew-symmetric part of the velocity gradient). This is equivalent to the use of a Jaumann-type stress rate, yet the equations obtained are form-identical to a small strain formulation [6]. Consequently, all the tensor variables below are rotation-compensated with respect to this frame.

2.1. Constitutive model framework

We consider elastic-plastic, anisotropic materials, defined by the following equations:

Yield function: $F(\sigma,\boldsymbol{X},R) := \sigma^{eq}(\sigma'-\boldsymbol{X}) - Y_0 - R$ (1)

where σ is the stress tensor, σ' is its deviator, $\boldsymbol{X}$ and R are the internal variables describing the current position ($\boldsymbol{X}$; back-stress) and size increase (R) of the yield surface. The material becomes plastic when the yield function vanishes. Y_0 is the initial size of the yield surface.

Flow rule: we consider associated plasticity:

$$\boldsymbol{D}^p = \dot{\lambda}\boldsymbol{V} \quad ; \quad \boldsymbol{V} = \partial F / \partial \boldsymbol{\sigma} \tag{2}$$

where $\boldsymbol{D}^p$ is the plastic strain rate, $\boldsymbol{V}$ is the gradient of the yield function and $\dot{\lambda}$ the plastic multiplier.

Hardening is governed by rate equation having the generic form below:

$$\dot{R} = H_R\dot{\lambda} \quad ; \quad \dot{\boldsymbol{X}} = \boldsymbol{H}_X\dot{\lambda}, \tag{3}$$

with the initial conditions $R(0) = 0$ and $\boldsymbol{X}(0) = \mathbf{0}$.

Hypo-elastic law: $\dot{\boldsymbol{\sigma}} = \boldsymbol{C} : (\boldsymbol{D} - \boldsymbol{D}^p)$, (4)

where $\boldsymbol{C}$ is the fourth order tensor of elastic constants and $\boldsymbol{D}$ is the total strain rate.

Tangent modulus: The plastic multiplier is computed using the consistency condition $\partial F/\partial t=0$. After differentiation of eq. (1) and use of equations (2-4), one can write the plastic multiplier as:

$$\dot{\lambda} = (\alpha / a)\boldsymbol{V} : \boldsymbol{C} : \boldsymbol{D}, \tag{5}$$

where $$a = \boldsymbol{V} : \boldsymbol{C} : \boldsymbol{V} + \boldsymbol{V} : \boldsymbol{H}_X + H_R$$

This expression can be used whatever the particular yield surface and the hardening laws considered. Then, the elastic-plastic tangent modulus $\boldsymbol{L}$ can be derived:

$$\boldsymbol{L} = \boldsymbol{C} - (\alpha / a)[(\boldsymbol{C} : \boldsymbol{V}) \otimes (\boldsymbol{V} : \boldsymbol{C})], \tag{6}$$

where α equals 1 for a plastic state and 0 otherwise.

So far, the material model has been developed in a general analytical framework. The yield function is defined by the equivalent stress σ^{eq} and its derivatives $\boldsymbol{V}$, while the hardening is defined by H_R and $\boldsymbol{H}_X$. Actually, all hardening variables (denoted by the pseudo-vector $\boldsymbol{y}$) are governed by rate equations of the type:

$$\dot{\boldsymbol{y}} = \boldsymbol{H}\dot{\lambda} \tag{7}$$

Thus, a time integration scheme can be built in this framework, whatever the particular hardening model or yield function.

2.2. Hardening models

By now, only quadratic yield surfaces are considered in this work:

$$\overline{\sigma} = \sqrt{(\boldsymbol{\sigma}' - \boldsymbol{X}) : \boldsymbol{M} : (\boldsymbol{\sigma}' - \boldsymbol{X})} \tag{8}$$

where $\boldsymbol{M}$ is a fourth order tensor of anisotropy coefficients. The well known von Mises and Hill'48 surfaces are particular cases of this function.

The interest of the modelling framework set in the former paragraphs is that available hardening models can be easily fitted into it. It has been shown that changing the yield surface consists in changing the definition of the equivalent stress and of its first derivative $\boldsymbol{V}$. Similarly, changing the hardening model in this framework consists simply in defining the two terms H_R and $\boldsymbol{H_X}$. Instead of describing the model equations, we simply give below, in a compact form, the definition of these terms for three well known material models. The first two are the classically used power law and saturating isotropic and kinematical model [1]. The third one is a physically-motivated, microstructure based hardening model especially developed for sheet forming applications [2,9].

Table 1. Hardening models, cast in the current formulation

Hardening model	Isotropic hardening term H_R	Kinematical hardening term $\boldsymbol{H_X}$
Swift, power-law	$H_R = nK^{\frac{1}{n}} R^{\frac{n-1}{n}}$	–
Armstrong-Frederick, saturating [1]	$H_R = C_R\,(R_{sat} - R)$	$\boldsymbol{H}_X = C_X\,(X_{sat}\,\boldsymbol{N} - \boldsymbol{X})$
Teodosiu-Hu, microstructure-based [9]	$H_R = \frac{f}{\lvert\mathbf{S}\rvert}\left(S_D H_{SD} - \lvert\mathbf{S}_L\rvert\lvert\mathbf{H}_{SL}\rvert\right) + H_v$ where: $H_V = C_R\,(R_{sat} - R_v)$ $H_{SD} = C_{SD}[g(S_{sat} - S_D) - hS_D]$ $\boldsymbol{H}_{SL} = -C_{SL}\,(\lvert\boldsymbol{S}_L\rvert / S_{sat})^n\,\boldsymbol{S}_L$ g and h defined as in [9]; *f, r, n, C_R, C_{SD}, C_{SL}, C_P etc. are material parameters*	$\boldsymbol{H}_X = C_X\,(X_{sat}\,\boldsymbol{n} - \boldsymbol{X})$ where $\boldsymbol{n} = (\boldsymbol{\sigma}' - \boldsymbol{X}) / \sigma^{eq}$ $\boldsymbol{N} = \mathbf{V} / \lvert\mathbf{V}\rvert$ $X_{sat} = X_0 + (1-f)\lvert\mathbf{S}\rvert\sqrt{r + (1-r)\frac{S_D^2}{\lvert\mathbf{S}\rvert^2}}$

Details on the different models are given in the corresponding references. It is expected that a much larger range of existing or to come hardening models fit this simple formulation, which appears very suitable for fast implementation into FE codes. In the following, we focus our attention on the last model, which is not currently available in commercial FE codes. Our intent is to asses the feasibility of its numerical implementation and its impact on the process simulation, especially spring-back.

3. Numerical implementation

3.1. Time integration algorithm

In finite element simulations, implicit integration is strongly recommended, for accuracy and stability considerations [8]. Explicit time integration is however much more simple to implement in a versatile way since no differentiation of the material model is required. In order to prevent extremely small time steps, we implemented a fourth order Runge-Kutta (RK4) time integration scheme [4]. In fact, a single algorithm has been built which implements the forward Euler and the 2nd and 4th order Runge-Kutta rules, as follows:

0) Input: Δt, $\Delta\varepsilon$, $\boldsymbol{y}_t$
1) $\Delta\boldsymbol{y}_0 = \boldsymbol{0}$
 For i=1 to N
2) Compute $\boldsymbol{H}$, $\Delta\lambda$, $\boldsymbol{L}$
3) $\Delta\boldsymbol{y}_i = \boldsymbol{H}(t + a_i\Delta t, \boldsymbol{y}_t + a_i\Delta\boldsymbol{y}_{i-1})\Delta\lambda_i$
 End loop
4) $\boldsymbol{y}_{t+\Delta t} = \boldsymbol{y}_t + \sum_{i=1}^{N} b_i\Delta\boldsymbol{y}_i$

$$\boldsymbol{L} = \sum_{i=1}^{N} b_i\boldsymbol{L}_i$$

5) Return,

where N = 1, 2 or 4 while a_i and b_i are constant coefficients. The result is the updated state variables vector $\boldsymbol{y}$ and the algorithmic tangent modulus $\boldsymbol{L}$. At step 2) of the algorithm, the following calculations are performed (N times):

0) Input: Δt, $\Delta\varepsilon$, $\boldsymbol{y}$
1) $F = \sigma^{eq}(\sigma' \text{-} \boldsymbol{X}) - Y_0 - R$
2) $\beta = \boldsymbol{V} : \Delta\varepsilon$
 If F<0 or β<0, elastic increment:
3) $\Delta\boldsymbol{y} = \boldsymbol{0}$; $\Delta\sigma = \boldsymbol{C} : \Delta\varepsilon$
 Else, elastic-plastic increment:
4) Compute $\boldsymbol{H} = (H_R, \boldsymbol{H}_X,..)$, $\dot{\lambda}$, $\boldsymbol{L}$
5) $\Delta\lambda = \dot{\lambda}\Delta t$
 $\Delta\boldsymbol{y} = \boldsymbol{H}\,\Delta\lambda$
 $\Delta\sigma = \boldsymbol{C} : (\Delta\varepsilon - \Delta\varepsilon^p)$
 End if
6) Return

where $\dot{\lambda}$ and $\boldsymbol{L}$ are computed using eqs. (5-6).

3.2. Accuracy of the integration scheme

A simple accuracy analysis has shown [5] that strain increments of $10^{-6}\ldots10^{-5}$ are required for the forward Euler scheme (when using constant time steps). The RK4 scheme reasonably allows for strain

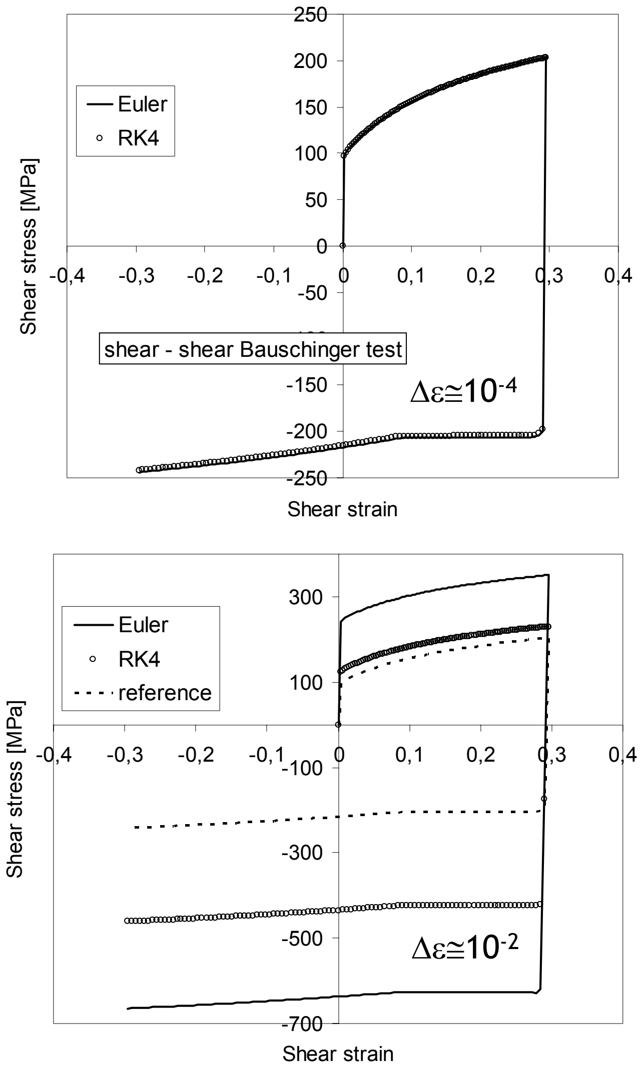

Figure 1. Accuracy of one element simulations of Bauschinger shear test, using two different strain increments.

increments of 10^{-4}. Nevertheless, the impact of the step size on accuracy strongly depends on the slope variation of the stress-strain curve. An adaptive time step control procedure can reduce again the required number of increments by an order of magnitude, performing very small steps only at the elastic-to-plastic transition. This can be very promising for single material point calculations; nevertheless, in FE simulation each point gets plastic at different moments thus reducing the interest of this strategy. As an example, the results of two different simulations, with different strain increments, are plotted in the figure 1. Constant step have been used, thus the elastic-to-plastic transition induces the whole error of the simulation.

3.3. Simulation of rheological tests

The soundest characteristic of the Teodosiu-Hu model is its ability to accurately simulate the transient zone after strain-path change. For illustration, consider two extreme cases: a strain reversal in shear test (Bauschinger effect) and a tensile test followed by a shear test in the same direction – e.g. the rolling direction (orthogonal test). Figure 2 depicts the result of the simulations for two sheet steels investigated in [2].

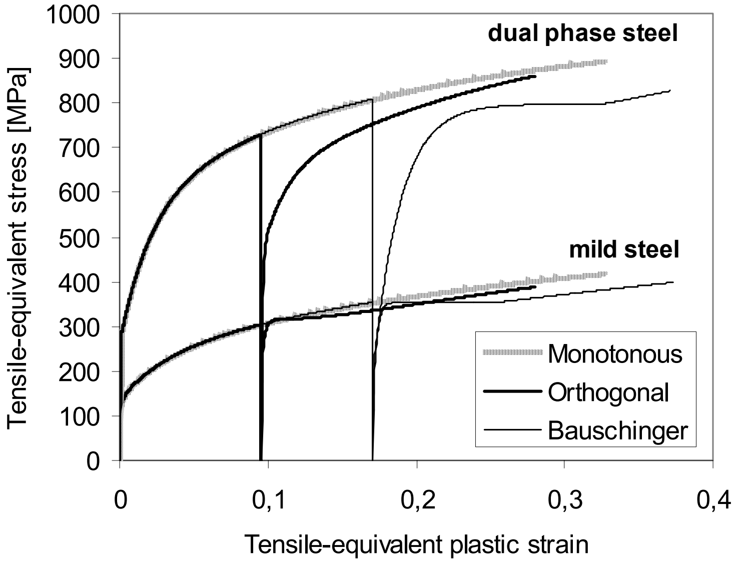

Figure 2. Simulation of two-step rheological tests. First step is tensile test (for orthogonal) or shear test (for Bauschinger) while the second one is shear test (forward or reverse, respectively).

The mechanical response of the two materials shows several differences. The difference in flow stress level is obvious and any hardening model should reproduce it. Also the onset of the Bauschinger effect (decrease of the flow stress at strain reversal) is modelled by kinematical hardening. Furthermore, the transient zone after strain reversal exhibits a plateau followed by hardening recovery. The amount of strain corresponding to the transient zone is very different for the two materials. Also, the orthogonal test induces two very different behaviours. These predictions have been shown to be very close to experimental results [2].

Spring-back simulations (among other) are expected to be very sensitive to such behaviour characteristics. Not only the flow stress level is proportional to the subsequent elastic strains, but tool removal also implies a drastic strain-path change. In several cases, small plastic strains can still occur during this process step; these plastic strains will belong in the transient zones and thus strongly differ from a material to another.

3.4. Finite element spring-back simulation

The constitutive algorithm has been implemented in both the dynamic explicit and the static implicit versions of the Abaqus software. The static implicit Abaqus/Standard version has been used for the simulation of the deep drawing of a U-shaped channel. This test has been introduced at Numisheet'93 for spring-back investigation purposes. The two materials are considered, combined with three blank-holding forces: 600 kN, 300 kN and 10 kN. The deformed shape, after tools removal, is plotted in figure 3 for all the simulations. The simulations are performed using two layers of solid, 2D, plane strain linear elements in the thickness of the sheet.

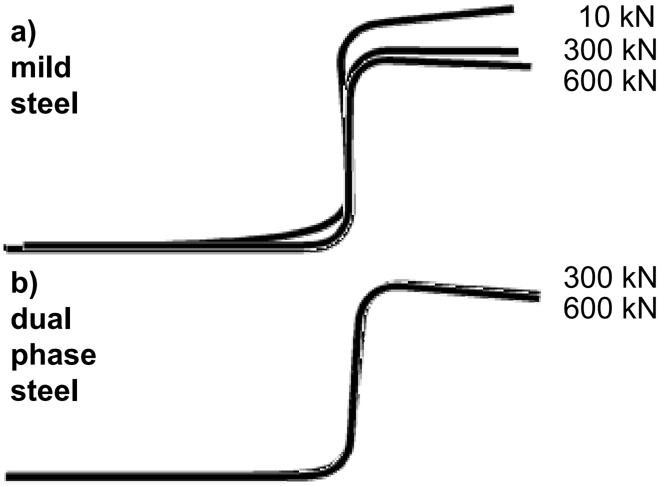

Figure 3. FE simulations of the U-shape deep drawing. Deformed shapes after spring-back. Due to symmetry, only the right-hand side is plotted.

As expected, the material behaviour has a determinant influence on spring-back. For mild steels, the die-radius angle appears more subject to spring-back, while for the dual phase it is the punch-radius angle. Also, the spring-back depends more on the holding force in the case of mild steel. The 10 kN force is too low for the DP steel and the simulation diverges for contact simulation reasons.

4. Conclusions

The explicit time integration schemes investigated in this work have several interesting advantages. The implementation of virtually any material model is easily possible. Provided small strain increments, the accuracy of the RK4 integration scheme seems acceptable even for delicate simulations like spring-back. It is even more interesting for single material point simulations (e.g. for micro-macro simulations). Such an implementation technique can be useful for rapid investigation of the benefits of a new model, before a more challenging implicit implementation is started.

Future work will concern the coupling of the hardening model with other yield surfaces (e.g. Barlat-type) and the development of an implicit integration scheme.

5. References

[1] Armstrong, P.J., Frederick, P.O.: Technical Report RD/B/N731, CEGB (1966).
[2] Bouvier, S., Teodosiu, C., Haddadi, H., Tabacaru, V.: Proc. EMMC6-MECAMAT, Liège (2002) 329.
[3] Chaboche, J.L., Cailletaud, G.: Comp. Methods. Appl. Mech. Engng. **133** (1996) 125.
[4] Cash, J.R., Karp, A.H.: ACM Trans. on mathematical software, **16** (1990) 201.
[5] Haddad, A., Balan, T., Abed-Meraim, F.: Proc. Esaform 2003, Salerno (2003) 187.
[6] Hughes, T.J.R., Winget, J.: Int. J. Num. Methods Engng. **15**-12 (1980) 1862.
[7] Li, K.P., Carden, W.P., Wagoner, R.H.: Int. J. Mech. Sci. **44** (2002) 103.
[8] Ortiz, M., Popov, E.P.: Int. J. Num. Methods Engng. **21** (1958) 1561.
[9] Teodosiu, C., Hu, Z.: Proc. 19th Riso Int. Symp. on Materials Science, Roskilde

(1998) 149.

Acknowledgements

The authors thank Dr. Xavier Lemoine from Arcelor R&D for his scientific contribution and financial support. The study has been funded by the European Commission thru the RFCS Contract No. 7210-PA/371. The first author is grateful to Prof. Cristian Teodosiu from LPMTM, University Paris XIII for scientific guidance on several topics used in this project.